

# Blinking statistics of a molecular beacon triggered by end-denaturation of DNA

**Tobias Ambjörnsson and Ralf Metzler**

NORDITA – Nordic Institute for Theoretical Physics,  
Blegdamsvej 17, DK-2100 Copenhagen Ø, Denmark

E-mail: ambjorn@nordita.dk, metz@nordita.dk

**Abstract.** We use a master equation approach based on the Poland-Scheraga free energy for DNA denaturation to investigate the (un)zipping dynamics of a denaturation wedge in a stretch of DNA, that is clamped at one end. In particular, we quantify the blinking dynamics of a fluorophore-quencher pair mounted within the denaturation wedge. We also study the behavioural changes in the presence of proteins, that selectively bind to single-stranded DNA. We show that such a setup could be well-suited as an easy-to-implement nanodevice for sensing environmental conditions in small volumes.

PACS numbers: 87.15.-v, 05.40.-a, 82.37.-j, 87.14.Gg

## 1. Introduction

During the last decade or so, technical progress in detection and manipulation of single molecules and their dynamics has snowballed. By fluorescence spectroscopy, optical tweezers, atomic force microscopy, or patch clamp techniques, for instance, it is possible on the single molecule level to probe the opening and closing dynamics of local denaturation zones in a DNA molecule [1], to study the binding of single-stranded DNA binding proteins to overstretched DNA [2, 3], to stepwise disrupt domains in a protein [4], or to monitor the passage of a biopolymer through a nanopore in a membrane [5, 6], just to name a few. This experimental progress is accompanied by advances in the theoretical understanding of fundamental processes relevant on small scales such as the Jarzinsky relation connecting measurements of the nonequilibrium work needed, e.g., to stretch an RNA segment [7], to the difference in the corresponding thermodynamic potential [8]; or the entropy production along single trajectories exposed to stochastic forces [9]. Given the novel possibilities to synthesize supramolecules with topologically confined mechanical units [10], entropy-based designer molecules such as molecular muscles were proposed [11, 12], and new possibilities to produce dynamic nanosensors discussed [13].

In what follows, we explore the dynamics of a stretch of double-stranded DNA (dsDNA), that is clamped at one end but allowed to denature from the other, as sketched in Figure 1. Internal bubble formation, in comparison, is suppressed by a

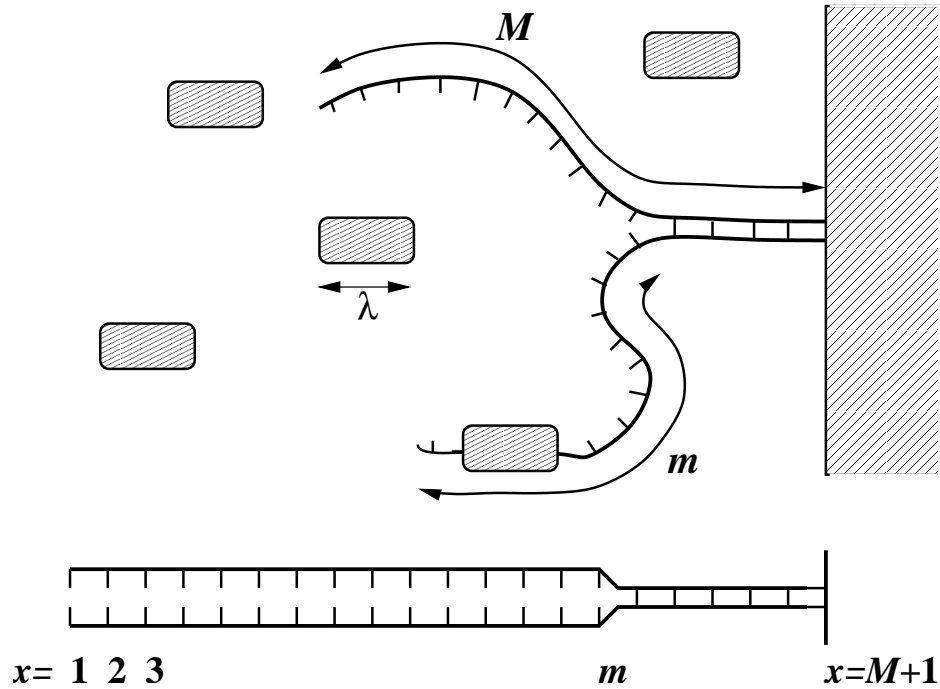


**Figure 1.** Schematic of the end-denaturing of a double-stranded DNA molecule, that is clamped at one end; here, by attachment to a wall. The number of denatured base-pairs is  $m$ , and the overall length of the DNA segment is  $M$ . Selectively single-stranded DNA binding proteins from the surrounding solution bind to the denatured portion of the DNA. Once bound, the SSBs prevent closing of the denaturation wedge. In reality, the clamping can be achieved by sealing the denaturation zone created by AT base-pairs with a stretch of more stable GC base-pairs, compare reference [1].

Boltzmann factor  $\sigma_0 \simeq 10^{-5} \dots 10^{-3}$  [14], and this effect can therefore be neglected, see below. In the setup we have in mind an individual base-pair is tagged with a fluorophore-quencher pair, see Figure 2: Once separated, the dye starts to fluoresce, and the resulting blinking can be detected [15]. Our aim is to establish a quantitative description of such a *molecular beacon*. We will use a master equation approach to describe the sequential unzipping and zipping dynamics of the denaturation wedge, also taking into account the possible presence of proteins, that selectively bind to single-stranded DNA (ssDNA). These single-stranded DNA binding proteins (SSBs) occur in the cells of most organisms. Here, we show that the autocorrelation function for the blinking depends on the concentration of SSBs and the binding strength between the single strand and the SSBs (the latter varies, for instance, with salt concentration) as well as temperature. The denaturation wedge depicted in figure 2 therefore acts as a nanosensor that can be probed on the single molecule level using fluorescence techniques.

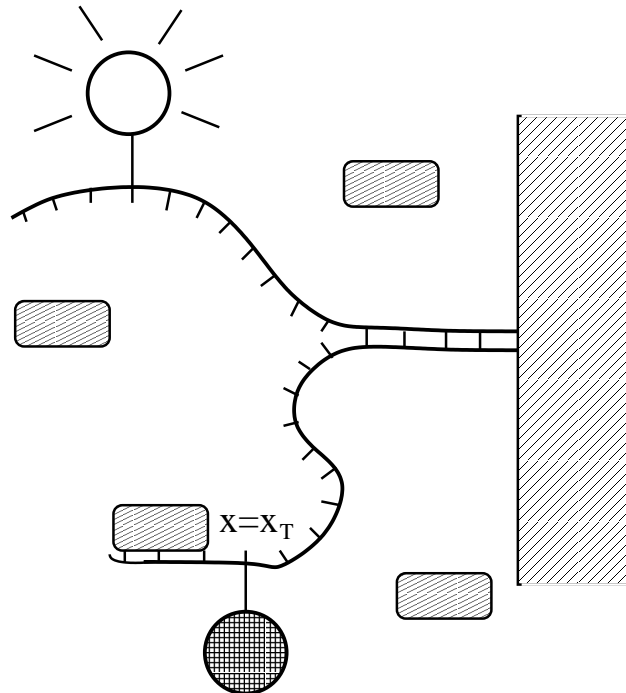


**Figure 2.** Schematic of the molecular beacon setup. A fluorophore starts to fluoresce in the incident laser light, once the denaturation wedge moves the fluorophore apart from the quencher.

## 2. Experimental setup: Quantifying the blinking dynamics of the molecular beacon

Before setting out to describe our general theoretical scheme, we first describe the experimental setup we have in mind in some detail. We consider modelling the blinking behaviour of a fluorophore-quencher pair mounted on the denaturation wedge as shown in Figure 2. This setup, similar to the ones described in References [1, 15] works as follows. As long as the dsDNA is intact, fluorophore and quencher are in close proximity. Once they come apart from one another when the denaturation wedge opens up, the incident laser light causes fluorescence of the dye. The on/off blinking of this "molecular beacon" can be monitored in the focus of a confocal microscope.

The blinking renders immediate information about the state of the base-pair, that is tagged by the dye-quencher pair. Blinking, that is, indicates that the base-pair is currently broken. It is therefore advantageous to define the random variable  $I(t)$  with the property

$$I(t) = \begin{cases} 0 & \text{if base-pair at } x = x_T \text{ is closed} \\ 1 & \text{if base-pair at } x = x_T \text{ is open} \end{cases}, \quad (1)$$

and we are interested in the behaviour of the autocorrelation function

$$A(t) = \langle I(t)I(0) \rangle - \langle I \rangle_{\text{eq}}^2, \quad (2)$$

where  $\langle I \rangle_{\text{eq}}$  is the (ensemble) equilibrium value. Given the fact that the formation of an internal denaturation bubble is connected with a rather high initiation barrier  $\sigma_0 \simeq 10^{-5} \dots 10^{-3}$  (corresponding to  $7 \dots 12 k_B T$  at room temperature), such bubbles are much less probable than denaturation from the unclamped end, we focus only on the end-denaturation. Therefore, a base-pair at  $x = x_T$  is open if  $m \geq x_T$ , see figure 2. A word on the interpretation of the average  $\langle I(t)I(0) \rangle$  is in order. Denoting by  $\rho(I, t; I', 0)$  the associated joint probability density that the tagged base-pair is in state  $I$  at time  $t$  given that it was in state  $I'$  at initial time  $t = 0$ , we can rewrite the autocorrelation function as

$$\langle I(t)I(0) \rangle = \sum_{I, I'} I \rho(I, t; I', 0) I' = \rho(1, t; 1, 0). \quad (3)$$

This is but the survival probability density for a denaturation wedge, i.e., the probability density that the base-pair is open at time  $t$ , given that it was open at system preparation at time  $t = 0$ .

In the remaining part of this study we present a general scheme for calculating the opening-and closing dynamics for the physical system presented in figures 1 and 2. The focus is on presenting a scheme which allows for the calculation of the measurable quantity  $A(t)$  defined above. We note, however, that our scheme is sufficiently general to allow for straightforward derivation of other experimental quantities, such as the binding dynamics of SSBs in optical tweezers overstretching setups [2, 3, 16]. In that case, the Boltzmann factor for opening a base-pair,  $u = \exp(\beta\epsilon)$  ( $\epsilon$  being the binding energy of a base-pair, see below) becomes modified to  $u = \exp(\beta\epsilon - \mathcal{T}\theta_0)$ , where  $\mathcal{T}$  is the external torque exerted by the optical tweezers setup, and  $\theta_0 = 2\pi/10.35$  is the relaxed dsDNA-twist per base-pair.

### 3. Master equation for end-unzipping

Denote by  $P(m, n, t)$  the probability distribution that there are  $m$  broken base-pairs and  $n$  bound SSBs at time  $t$ . As  $m$  and  $n$  are the slow variables of the system, their dynamics can be described in terms of the master equation

$$\begin{aligned} \frac{\partial P(m, n, t)}{\partial t} = & \mathbf{t}^+(m-1, n)P(m-1, n, t) + \mathbf{t}^-(m+1, n, t)P(m+1, n, t) \\ & - [\mathbf{t}^+(m, n) + \mathbf{t}^-(m, n)] P(m, n, t) \\ & + \mathbf{r}^+(m, n-1)P(m, n-1, t) + \mathbf{r}^-(m, n+1)P(m, n+1, t) \\ & - [\mathbf{r}^+(m, n) + \mathbf{r}^-(m, n)] P(m, n, t), \end{aligned} \quad (4)$$

compare the discussion in References [17, 18, 19]. Mediated by the transfer rates  $\mathbf{t}^\pm$  and  $\mathbf{r}^\pm$ , the population of a given state  $(m, n)$  is continuously changed by (un)zipping a further base-pair and (un)binding of an SSB. To complete the master equation (4), we need to specify the boundary conditions: The clamping to the right at base-pair  $x = M + 1$  ensures that no further unzipping beyond base-pair  $M$  occurs, namely,

$$\mathbf{t}^+(M, n) = 0. \quad (5)$$

Moreover, if both branches of the denaturation wedge are fully occupied by SSBs, i.e., the maximum number of SSBs,

$$n^{\max}(m) = 2 \left\lceil \frac{m}{\lambda} \right\rceil, \quad (6)$$

is bound, then the base-pair at the zipping fork is not allowed to close:

$$\mathbf{t}^- \left( m = \frac{n\lambda}{2}, n = n^{\max}(m) \right) = 0. \quad (7)$$

Also, if only one of the two branches of the wedge is fully occupied the zipper cannot close:

$$\mathbf{t}^- \left( m = \frac{(n+1)\lambda}{2}, n = n^{\max}(m) - 1 \right) = 0. \quad (8)$$

Similar to the (un)zipping rates  $\mathbf{t}^\pm$ , we impose the boundary condition

$$\mathbf{r}^+(m, n^{\max}(m)) = 0, \quad (9)$$

i.e., once the denaturation wedge is completely occupied, no additional SSB is allowed to bind; and when  $n = 0$  SSBs are bound, no further SSB can detach:

$$\mathbf{r}^-(m, 0) = 0, \quad (10)$$

The configuration lattice showing the allowed moves is illustrated in Figure 3. Empty arrow heads indicate forbidden moves.

The general solution of the master equation (4) can be obtained through the ansatz

$$P(m, n, t) = \sum_p c_p Q_p(m, n) e^{-\eta_p t}, \quad (11)$$

corresponding to an expansion in eigenmodes. Here, the expansion coefficients  $c_p$  are determined by the initial condition. Inserting above expansion into equation (4) produces the eigenvalue equation

$$\begin{aligned} -\eta_p Q_p(m, n) = & \mathbf{t}^+(m-1, n) Q_p(m-1, n) + \mathbf{t}^-(m+1, n) Q_p(m+1, n) \\ & - [\mathbf{t}^+(m, n) + \mathbf{t}^-(m, n)] Q_p(m, n) \\ & + \mathbf{r}^+(m, n-1) Q_p(m, n-1) + \mathbf{r}^-(m, n+1) Q_p(m, n+1) \\ & - [\mathbf{r}^+(m, n) + \mathbf{r}^-(m, n)] Q_p(m, n) \end{aligned} \quad (12)$$

for the  $p$ th eigenmode. The concrete forms for the transfer rates are defined in the next section.

#### 4. Partition function and transfer rates

In order to obtain the transfer coefficients  $\mathbf{t}^\pm$  and  $\mathbf{r}^\pm$ , we first define the partition function  $\mathcal{Z}(m, n)$  for the end-denaturation fork of the dsDNA and the SSBs bound to its two branches. To this end, we note that we can decouple the partition coefficient

$$\mathcal{Z}(m, n) = \mathcal{Z}^{\text{DNA}}(m) \mathcal{Z}^{\text{SSB}}(m, n) \quad (13)$$

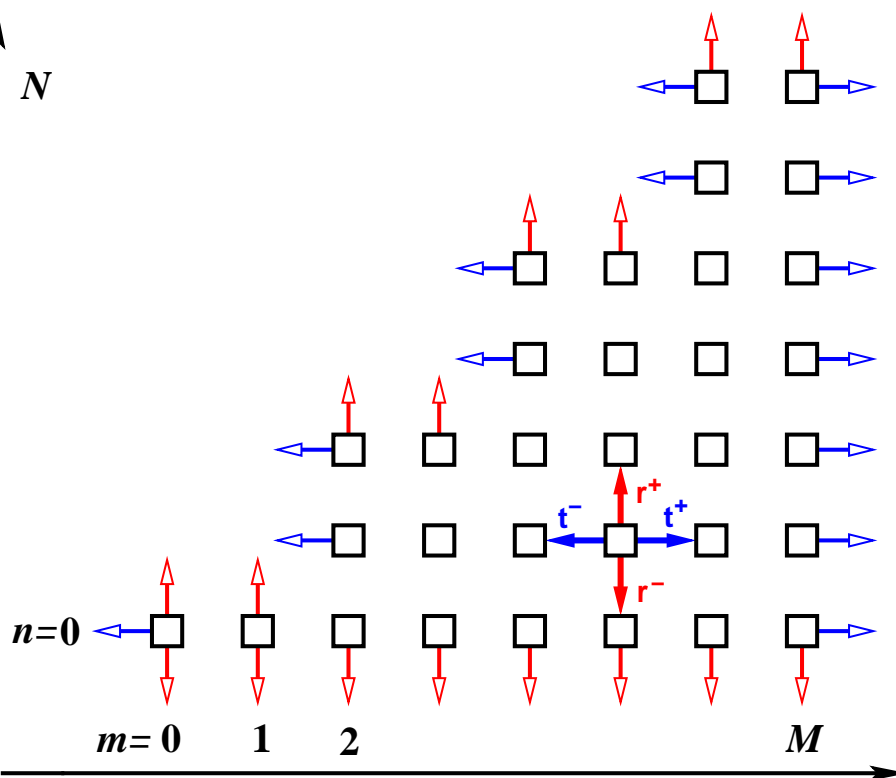


**Figure 3.** Configuration lattice showing the possible configurations  $\square$  of the system in the  $(m, n)$ -plane. The empty arrow heads represent forbidden moves due to the boundary conditions. The maximum number of bound SSBs is  $N = 2[M/\lambda]$ .

into the contributions  $\mathcal{Z}^{\text{DNA}}$  counting the degrees of freedom of the DNA molecule, and the contribution  $\mathcal{Z}^{\text{SSB}}$  of the SSBs. According to the Poland-Scheraga model of DNA denaturation, we have

$$\mathcal{Z}^{\text{DNA}}(m) = u^m. \quad (14)$$

Here,  $u = \exp(\beta\epsilon)$  is the Boltzmann factor for opening a base-pair, i.e., the activation needed to overcome the free energy barrier  $\epsilon$  for opening an additional base-pair.  $\epsilon$  combines two appreciable contributions from enthalpy cost and entropy gain on breaking the base-pair, that almost cancel such that  $\epsilon$  is of the order of a  $k_B T$  at physiological temperature and salt: At  $37^\circ$ ,  $u \approx 0.6$  in a zone of AT base-pairs, and  $u \approx 0.2$  in a GC-domain [14]. We note that the parameter  $u$  is sensitive to salt concentration. Here, we consider homopolymer zones of either AT or GC; for the treatment of a heteropolymer, see Reference [20]. As already mentioned, we also neglect the formation of internal denaturation bubbles within the dsDNA stretch, that would require the crossing of the initiation barrier  $\sigma_0$ . This contrasts our previous studies [21, 17, 18, 20, 22], in which we focused on internal bubbles, preventing end-denaturation wedges by clamping at both ends. Note also that in the case of the end-wedges, we do not have to take care of the entropy loss due to loop formation as present in internal denaturation bubbles.

The contribution from the SSBs has the form

$$\mathcal{Z}^{\text{SSB}}(m, n) = \kappa^n \Omega^{\text{SSB}}(m, n), \quad (15)$$

sharing the energetic component

$$\kappa = c_0 K^{\text{eq}} \quad (16)$$

per bound SSB, where  $c_0$  is the SSB concentration in solution and  $K^{\text{eq}} = v_0 \exp(|E_{\text{bind}}|/k_B T)$  the equilibrium binding constant of SSB-binding, with the typical volume  $v_0$  of the SSBs and the binding energy  $E_{\text{bind}}$ ; and the number of possible ways of arranging  $n$  SSBs on the two arches of the denaturation fork, both being of length  $m$  [17, 18]:

$$\Omega^{\text{SSB}}(m, n) = \sum_{n'=0}^n \omega^{\text{SSB}}(m, n') \omega^{\text{SSB}}(m, n - n') \Bigg|_{\substack{n-n' \leq n^{\text{max}}/2 \\ n' \leq n^{\text{max}}/2}}. \quad (17)$$

This counting allows to have a different number of SSBs on the two arches. The degrees of freedom of distributing  $n$  SSBs each covering  $\lambda$  bases, on an arch of size  $m$  is

$$\omega^{\text{SSB}}(m, n) = \binom{m - (\lambda - 1)n}{n} = \frac{(m - [\lambda - 1]n)!}{n!(m - \lambda n)!}. \quad (18)$$

From the partition function, we can now come to specify the transfer rates. As a first requirement we impose that the rates obey the detailed balance condition [23]

$$\mathbf{r}^+(m, n - 1) \mathcal{Z}(m, n - 1) = \mathbf{r}^-(m, n) \mathcal{Z}(m, n) \quad (19)$$

for SSB (un)binding, and

$$\mathbf{t}^+(m - 1, n) \mathcal{Z}(m - 1, n) = \mathbf{t}^-(m, n) \mathcal{Z}(m, n) \quad (20)$$

for base-pair (un)zipping. Detailed balance guarantees that the probability distribution  $P(m, n, t)$  for long times relaxes towards the Boltzmann distribution. However, the detailed balance condition does not uniquely specify the rates. Using the remaining freedom of choice [23, 17], we settle for the following forms. In the case of SSB (un)binding, we choose

$$\mathbf{r}^+(m, n) = (n + 1)q \frac{\mathcal{Z}(m, n + 1)}{\mathcal{Z}(m, n)} = (n + 1)q\kappa \frac{\Omega^{\text{SSB}}(m, n + 1)}{\Omega^{\text{SSB}}(m, n)} \quad (21)$$

for the binding rate, and

$$\mathbf{r}^-(m, n) = nq \quad (22)$$

for unbinding. The unbinding rate, that is, is proportional to the number of bound SSBs, as it should. Apart from this  $n$ -factor, we choose it to solely depend on the constant unbinding rate  $q$ . Conversely, the binding rate includes, apart from this rate  $q$ , the binding strength  $\kappa$ , the relative number of degrees of freedom given by the ratio of the  $\Omega^{\text{SSB}}$  factors; and the factor  $(n + 1)$ . The factor  $(n + 1)\Omega^{\text{SSB}}(m, n + 1)/\Omega^{\text{SSB}}(m, n)$  accounts for the combinatorial number of ways to put an additional SSB of size  $\lambda$  onto either arch of the denaturation fork. In the limit  $\lambda = 1$  the resulting expression

for  $r^+(m, n)$  becomes  $q\kappa(m - n)$  and thus designates the number of free binding sites, compare the discussion in [17, 23].

Similarly, we choose a completely asymmetric form for the base-pair (un)zipping rates. Thus, for unzipping of an additional base-pair we use ‡

$$t^+(m, n) = t^+(m) = k \frac{\mathcal{Z}^{\text{DNA}}(m + 1, n)}{\mathcal{Z}^{\text{DNA}}(m, n)} = ku, \quad (23)$$

carrying the full Boltzmann factor  $u$ , apart from the rate constant  $k$ . The zipping rate

$$t^-(m, n) = k \frac{\mathcal{Z}^{\text{DNA}}(m - 1, n)}{\mathcal{Z}^{\text{DNA}}(m, n)} = k \frac{\Omega^{\text{SSB}}(m - 1, n)}{\Omega^{\text{SSB}}(m, n)} \quad (24)$$

contains all information related to the interplay with the number  $m$  of bound SSBs, and is proportional to the probability that the base-pair next to the denaturation fork is unoccupied. This choice realistically describes the fact that a region almost fully occupied with SSBs is less likely to decrease in size. We note that in general  $t^-(m, n) \leq k$ , and that  $t^-(m, 0) = k$ . Note also that we can conveniently define a dimensionless parameter

$$\gamma \equiv \frac{q}{k} \quad (25)$$

that measures the competition between SSB (un)binding and base-pair (un)zipping.

## 5. Results: Blinking autocorrelation of the molecular beacon

Having defined the dynamics of the end-denaturation wedge in terms of the numbers of broken base-pairs,  $m$ , and of bound SSBs,  $n$ , we now proceed to calculate the autocorrelation  $A(t)$  for the blinking behaviour of a fluorophore-quencher pair mounted on the denaturation wedge as shown in Figure 2. Following the results from reference [20], we can express  $A(t)$  according to equation (2) in the form

$$A(t) = \sum_{p \neq 0} T_p^2 e^{-t/\tau_p}, \quad (26)$$

with relaxation times  $\tau_p \equiv \eta_p^{-1}$ , and where

$$T_p = \sum_{m, n} Q_p(m, n) \Big|_{m \geq x_T}. \quad (27)$$

It should also be noted that, in order to be detected experimentally, it might be necessary that the fluorophore-quencher pair should be separated further than by the separation provided by solely opening the base-pair  $x_T$ . Thus, if  $\Delta$  additional base-pairs need to be broken before fluorescence occurs, the quantity  $T_p$  will be modified to

$$T_p = \sum_{m, n} Q_p(m, n) \Big|_{m \geq x_T + \Delta}.$$

‡ We here, for simplicity, neglect any  $m$ -dependence of the rate constant  $k$ , compare the discussion about the 'hook'-effect in references [17, 18].



Alternatively, we can rewrite the autocorrelation function  $A(t)$  according to the spectral decomposition

$$A(t) = \int_0^\infty f(\tau) \exp\left(-\frac{t}{\tau}\right) d\tau. \quad (28)$$

This way, we obtain the weighted spectral density ("relaxation time spectrum")

$$f(\tau) = \sum_{p \neq 0} T_p^2 \delta(\tau - \tau_p). \quad (29)$$

This distribution  $f(\tau)$  renders information about the contributions of individual relaxation modes to the autocorrelation function  $A(t)$ , see also below.

For the two limiting cases corresponding to absence of SSBs, and to fast (un)binding dynamics of the SSBs, we obtain analytical solutions for  $A(t)$  from the master equation (4) below. The general case is solved numerically along similar lines as developed in references [17].

### 5.1. Absence of SSBs

If no SSBs are present, the (un)zipping rates  $\mathbf{t}^\pm$  assume the simpler form

$$\bar{\mathbf{t}}^+(m) = \mathbf{t}^+(m, 0) = ku, \quad (30)$$

and

$$\bar{\mathbf{t}}^-(m) = \mathbf{t}^-(m, 0) = k, \quad (31)$$

corresponding the transfer rates for an asymmetric random walk. This contrasts the non-linear form for internal bubbles that includes the loop entropy loss [17, 18]. The master equation reduces to the one-variable form

$$\begin{aligned} \frac{\partial \bar{P}(m, t)}{\partial t} &= \bar{\mathbf{t}}^+(m-1) \bar{P}(m-1, t) + \bar{\mathbf{t}}^-(m+1) \bar{P}(m+1, t) \\ &\quad - [\bar{\mathbf{t}}^+(m) + \bar{\mathbf{t}}^-(m)] \bar{P}(m, t) \end{aligned} \quad (32)$$

with the eigenvalue decomposition  $\bar{P}(m, t) = \sum_p \bar{c}_p \bar{Q}_p(m) e^{-\bar{\eta}_p t}$ . Thus, we obtain the eigenvalue equation

$$\begin{aligned} -\bar{\eta}_p \bar{Q}_p(m) &= \bar{\mathbf{t}}^+(m-1) \bar{Q}_p(m-1) + \bar{\mathbf{t}}^-(m+1) \bar{Q}_p(m+1) \\ &\quad - [\bar{\mathbf{t}}^+(m) + \bar{\mathbf{t}}^-(m)] \bar{Q}_p(m), \end{aligned} \quad (33)$$

with the obvious boundary conditions  $\bar{\mathbf{t}}^-(0) = 0$ , and  $\bar{\mathbf{t}}^+(M) = 0$ . The solution of the reduced eigenvalue equation for  $\bar{Q}_p$  can be obtained in terms of orthogonal polynomials (or Chebyshev polynomials) according to References [17, 24]:

$$\bar{Q}_p(m) = \frac{u^{m/2}}{\sin \omega_p} \left\{ \sin [(m+1)\omega_p] - u^{-1/2} \sin [m\omega_p] \right\}, \quad (34)$$

where the eigenvalues become

$$\bar{\eta}_p = k [u + 1 - 2u^{1/2} \cos \omega_p] \quad (35)$$

with

$$\omega_p = \frac{p\pi}{M+1}. \quad (36)$$

We notice that the relaxation times  $\bar{\tau}_p \equiv 1/\bar{\eta}_p$  fulfil the inequalities

$$\tau_{\min}(u) \equiv k^{-1} (1 + u^{1/2})^{-2} \leq \bar{\tau}_p \leq k^{-1} (1 - u^{1/2})^{-2} \equiv \tau_{\max}(u). \quad (37)$$

Thus, at the melting transition where  $u = 1$ , and for an infinitely long DNA segment  $M \rightarrow \infty$  the longest relaxation time diverges, i.e., the denaturation wedge has a diverging lifetime, as one would expect. The correlation function  $A(t)$  corresponding to the results above are shown by the black dash-dotted curves in figure 4.

We note that conditions similar to the absence of SSBs are fulfilled if the concentration of SSBs is very low,  $\kappa \rightarrow 0$ , or if  $\gamma\kappa \rightarrow 0$ , compare the existence of a kinetic block to SSB-binding in DNA-bubbles [2, 3, 17, 18].

### 5.2. Fast (un)binding dynamics of SSBs

In case the (un)binding dynamics of the SSBs is much faster than the typical base-pair (un)zipping rates,  $\gamma \gg 1$ , we can adiabatically eliminate the degrees of freedom corresponding to the SSB dynamics [25]. Ensuing are an effective free energy landscape, dressed by the SSB-interactions with the denaturation wedge, and a reduced one-variable master equation of the type (32), but with the following (dressed) rate coefficients [17]:

$$\tilde{\mathbf{t}}^{\pm}(m) = \sum_{n=0}^{n^{\max}(m)} \mathbf{t}^{\pm}(m, n) \frac{\mathcal{Z}(m, n)}{\mathcal{Z}(m)}, \quad (38)$$

where  $\mathcal{Z}(m) \equiv \sum_n \mathcal{Z}(m, n)$ . When calculating the two dressed rates  $\tilde{\mathbf{t}}^{\pm}$ , it is important to consider the boundary conditions (5), (7), and (8). From these we also deduce the modified boundary conditions  $\tilde{\mathbf{t}}^+(M) = 0$  and  $\tilde{\mathbf{t}}^-(0) = 0$ . The corresponding result for the autocorrelation function are shown by the dashed curves in figure 4.

### 5.3. General case

In the general case when the dynamics of SSB (un)binding and base-pair (un)zipping occur on comparable time scales,  $\gamma \sim 1$ , the eigenvalue equation (12) has to be solved numerically; for detailed elaboration on the procedure, see reference [17]. In figure 4, we display some typical examples for the relaxation time spectrum and the autocorrelation function for various values of SSB binding strength  $\kappa$  and rate ratio  $\gamma$ .

### 5.4. Discussion

We first note that the autocorrelation function  $A(t)$  in the semi-log plot is non-exponential, corresponding to a multimodal relaxation behaviour, that was also observed in experiment [1]. This is reflected in the rather broad distribution of relaxation times shown in figure 4. In the binned data for the relaxation times, the first bin contains the major portion of the relaxation contributions for all cases. This describes the relaxation

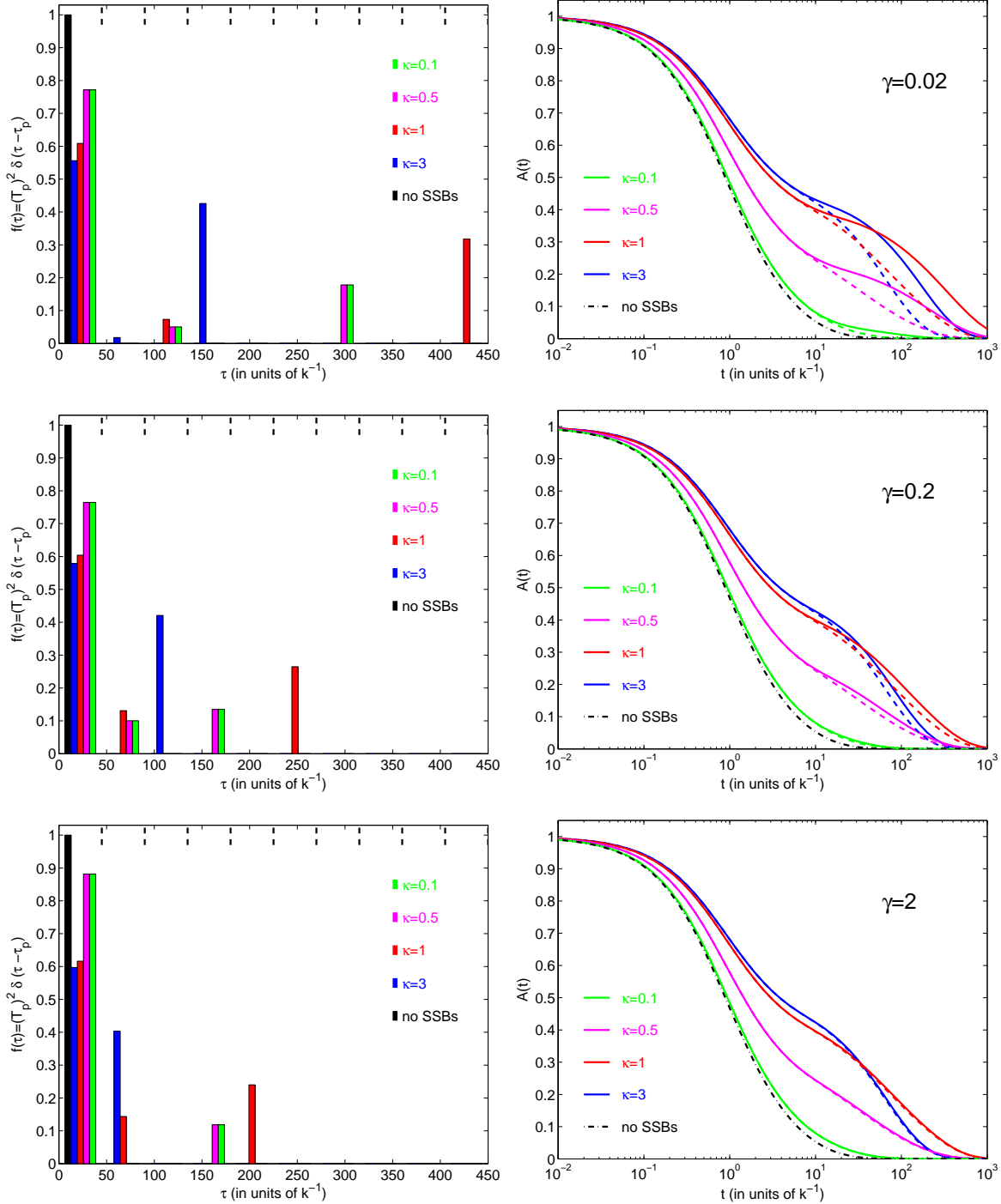


**Figure 4.** Relaxation time spectrum  $f(\tau)$  and autocorrelation function  $A(t)$  for different values of the binding strength  $\kappa$  and the ratio  $\gamma = q/k$  between the unbinding and the unzipping rate constants, as indicated in the graphs. The dashed curves correspond to the approximation of adiabatic elimination (fast binding). In the plots for the relaxation time spectra,  $f(\tau)$ , the data were binned (the black dashed lines at the top of the graphs show the bin size). We chose  $u = 0.6$ ,  $\lambda = 5$ ,  $x_T = 1$ , and  $M = 30$ . Notice that strongly binding SSBs increase the relaxation time by orders of magnitude (logarithmic abscissa in the  $A(t)$  plots).

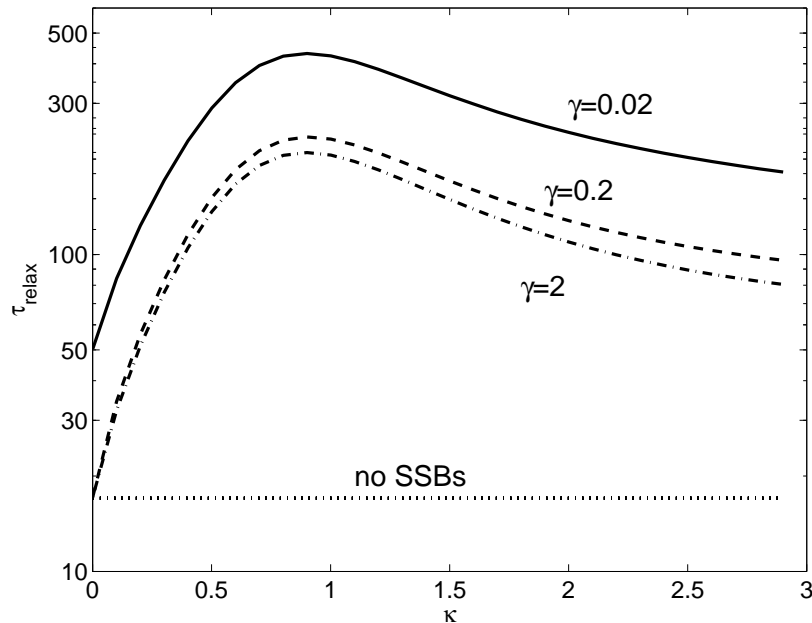


**Figure 5.** Longest relaxation time  $\tau_{\text{relax}}$  as a function of SSB binding strength  $\kappa$ . Note the dramatic variation of  $\tau_{\text{relax}}$  (logarithmic ordinate). We chose  $u = 0.6$ ,  $\lambda = 5$ , and  $M = 30$ . A maximum occurs at around  $\kappa = 1$ .

of the denaturation wedge itself, i.e., the relaxation due to the base-pair (un)zipping process. In the plots for  $A(t)$ , this corresponds to the first relaxation shoulder located at a few inverse zipping time units,  $k^{-1}$ .

In absence of SSBs, our coarse-grained plot of the relaxation time distribution shows only one contribution, corresponding to only one relaxation shoulder in the graphs for  $A(t)$ . With increasing binding strength  $\kappa$ , a second relaxation shoulder in  $A(t)$  is building up. This is due to the relaxation of SSB (un)binding. Let us discuss the somewhat involved behaviour for the various values of  $\kappa$  in the case  $\lambda = 1$ , for which the occupation fraction of SSBs on the ssDNA branches of the denaturation wedge becomes  $f = \kappa/(1 + \kappa)$  [19]. We see that  $\kappa = 1$  leads to an occupation fraction  $f = 1/2$ . In that case, we would expect the relaxation time for SSB occupation to be the longest. Both for increasing and decreasing  $\kappa$ , the fraction of vacancies and bound SSBs is decreasing, respectively, so that the exchange between both species becomes faster, and  $A(t)$  decays quicker than for  $\kappa = 1$ . However, for  $\kappa < 1$ , the number of bound SSBs is smaller and mostly a certain binding site is vacant, and the relaxation therefore quicker than for  $\kappa > 1$ , for which a site is mostly occupied. Indeed, these trends can be observed in the plotted examples: The relaxation time contribution is the longest in the case  $\kappa = 1$ . This observation is corroborated in figure 5 illustrating the behaviour of the longest relaxation time as function of binding strength  $\kappa$ : the maximum close to  $\kappa \approx 1$  is distinct.

In dependence of the ratio  $\gamma = q/k$  of rates  $q$  for SSB unbinding and  $k$  for base-pair unzipping, the increase in the relative speed,  $\gamma$ , of the SSB dynamics is immediately

evident from the shift towards shorter  $\tau$  in the relaxation time spectrum. In the plots for  $A(t)$ , the results in presence of SSBs approach the adiabatic approximation; in the case  $\gamma = 2$ , virtually no difference between the full result and the fast binding limit are visible in  $A(t)$ .

## 6. Conclusions

We investigated by means of a master equation approach in detail the dynamics of end-denaturation of a clamped stretch of homopolymer DNA. The transfer rates were obtained from the partition coefficients based on the Poland-Scheraga model of DNA denaturation. We chose the rates  $t^\pm$  and  $r^\pm$  for base-pair (un)zipping and SSB (un)binding, such that detailed balance is fulfilled, i.e., thermal equilibrium reached for long times. We furthermore chose these rates in a fully asymmetric form guaranteeing that base-pair unzipping is proportional to the Boltzmann factor for breaking the base-pair and the fundamental rate  $k$ . For base-pair zipping, the rate is given by  $k$  in absence of SSBs, whereas in presence of SSBs it gets dressed by the combinatorial ratio slowing down the zipping when SSBs are bound (essentially, by the probability that the base-pair next to the zipping fork is vacant), and preventing closing of the wedge once it is fully occupied. Similarly, we chose the (un)binding rates such that the unbinding is specified by the fundamental rate  $q$  times the number of bound SSBs. Binding is biased by the binding strength  $\kappa$  and the probability of adding another SSB to the two arches of the denaturation wedge.

Mounting a fluorophore-quencher pair at position  $x_T$  on either arch of the associated denaturation wedge, a molecular beacon is built, whose blinking dynamics, corresponding to the open or closed state of the base-pair  $x_T$ , is described by the random variable  $I$ . For this quantity, we obtained the autocorrelation function  $A(t)$  and the associated spectrum of relaxation times. The quantity  $A(t)$  can be measured directly in experiments (see, e.g., references [1, 15]). The predicted behaviour of  $A(t)$  and the spectrum  $f(\tau)$  shows a multimodal behaviour with two pronounced relaxation shoulders in the presence of SSBs. As our model involves physical parameters that are known for given solvent conditions ( $u, \kappa$ ) or can be determined independently ( $k, q$ ), our model becomes fully quantitative, and can be used to devise future experimental setups.

The molecular beacon setup we propose represents the basis for an interesting nanosensor. Constructing a small stretch of AT base-pairs and clamping them with a few GC base-pairs at one end (compare the construction used in reference [1]), such a nanosensor would be of the linear size of some 20 nm. A low concentration of such nanosensors would therefore be sufficient to probe for presence of SSBs, salt conditions, or similar, in small probe volumes as, for instance, encountered in gene arrays. The rather large changes in the relaxation time spectrum invoked by the presence of SSBs (or, by varying  $u$ , corresponding to temperature or salt changes, not shown here) corroborate that this kind of sensor could actually be rather sensitive. We note that instead of the conventional fluorophores, that bleach rather quickly, longer-lived quantum dots or

plasmon resonant nanoparticles are now available, see, for instance, references [26, 27].

Whereas our calculations are for a homopolymer denaturation zone, the simplest possibility in view of designing a nanodevice, it is possible to extend the model to a heterogeneous sequence, see reference [20]. However, the numerical evaluation of the corresponding master equation may become challenging, especially, when longer denaturation zones and small SSBs are employed. An efficient alternative for such more involved cases is provided by stochastic simulations techniques such as the Gillespie algorithm, as studied recently in the context of denaturation fluctuations in DNA [22].

## References

- [1] Altan-Bonnet G, Libchaber A and Krichevsky O 2003 *Phys. Rev. Lett.* **90** 138101
- [2] Pant K, Karpel RL and Williams MC 2003 *J. Mol. Biol.* **327** 571
- [3] Pant K, Karpel RL, Rouzina I and Williams MC 2004 *J. Mol. Biol.* **336** 851
- [4] Rief M, Gautel M, Oesterhelt F, Fernandez JM, Gaub HE 1997 *Science* **276** 1109
- [5] Kasianowicz J J, Brandin E, Branton D and Deamer D W 1996 *Proc. Natl. Acad. Sci. (USA)* **93**, 13770
- [6] Meller A 2003 *J. Phys. Cond. Mat.* **15** R581
- [7] Liphardt J, Dumont S, Smith SB, Tinoco Jr I and Bustamante C 2002 *Science* **296** 1832
- [8] Jarzynski C 1997 *Phys. Rev. Lett.* **78** 2690
- [9] Seifert U 2005 *Eprint cond-mat/0503686*
- [10] Lehn J-M 1995 *Supramolecular Chemistry* (Wiley-VCH, Weinheim)
- [11] Hanke A and Metzler R 2003 *Chem. Phys. Lett.* **359** 22
- [12] Bottari G, Dehez F, Leigh DA, Nash PJ, Perez EM, Wong JKY and Zerbetto F 2003 *Angew. Chem. Internat. Ed.* **42** 5886
- [13] Ambjörnsson T and Metzler R 2005 *J. Comput. Theor. Nanoscience* at press
- [14] Blake RD, Bizzaro JW, Blake JD, Day GR, Delcourt SG, Knowles J, Marx KA and SantaLucia Jr J 1999 *Bioinformatics* **15** 370
- [15] Krichevsky O and Bonnet G 2002 *Rep. Prog. Phys.* **65** 251
- [16] Sokolov IM, Metzler R, Pant K and Williams MC 2005 *Biophys. J.* **89** 895
- [17] Ambjörnsson T and Metzler R 2005 *J. Phys. Cond. Mat.* **17** S1841
- [18] Ambjörnsson T and Metzler R 2005 *Phys Rev. E Rapid Comm* at press
- [19] Ambjörnsson T and Metzler R 2004 *Phys. Biol.* **1** 77
- [20] Ambjörnsson T and Metzler R 2005 in preparation
- [21] Hanke A and Metzler R 2003 *J. Phys. A* **36** L473
- [22] Banik SK, Ambjörnsson T and Metzler R 2005 *Europhys. Lett.* **71** 852
- [23] van Kampen NG 1992 *Stochastic processes in physics and chemistry* (North-Holland Elsevier, Amsterdam)
- [24] Ledermann W and Reuter GEH 1954 *Phil. Trans. R. Soc. A* **246** 321
- [25] Risken H 1989 *The Fokker-Planck equation* (Springer-Verlag, Berlin)
- [26] Medintz IL, Clapp AR, Mattoussi H, Goldman ER, Fisher B and Mauro JM 2003 *Nature Materials* **2** 630
- [27] Shultz, DA 2003 *Curr. Opin. in Biotech.* **14** 13